Granular Matter
DOI 10.1007/s10035-010-0233-4

ORIGINAL PAPER

Structural properties of wet granular beds subjected to tapping

R. O. Uñac · A. M. Vidales

Received: 24 June 2010

Abstract Based on a simple numerical model for wet granular beds, we study the structural properties of wet particles subjected to tapping in terms of the global anisotropy and angular distribution presented by their contacts. The model allows to generate 2-dimensional packings of disks that can form capillary bridges due to the presence of interstitial liquid. A pseudodynamic simulation of adhesive hard disks has been implemented. The bed is subjected to a tapping-like excitation and we study the evolution of structural anisotropy of the packing with the number of taps. We also analyse the behavior of the angular distribution of contacts and anisotropy as a function of tapping intensity and liquid content. Present results help to better understand the behavior found in a previous work for the packing fraction of these systems. They also demonstrate that anisotropy alone not always helps to completely understand the behavior of the structural properties of wet particles.

Keywords Anisotropy · Hard disks · Capillary bridges · Pseudodynamics · Compaction · Tapping

1 Introduction

Although problems involving the presence of wet granular media have a long history in both the technological and industrial interest as in the basic science, little is yet known about the mechanisms that govern the mechanical behavior of these media. However, there are some studies that have laid the basis for the beginning of a systematic and detailed treatment of the main forces involved in the interaction between two wet grains [1,2].

The development of models for wet granular materials is still incipient but there has been a growing interest in the last years [3–8].

In [3] authors reported an experimental study for the packing of spherical particles with special reference to the effect of liquid addition. In particular, they discussed how dry based porosity increased to a maximum value and then remained constant with liquid content increase. They showed that the relationship between porosity and liquid content is mainly controlled by the properties of particles and liquid, specially, particle size and surface tension. The same experiments were performed for packings of multi-sized coarse spheres [4]. Here again, results indicated that, in addition to water content, porosity was also strongly affected by particle sizes and their distribution.

On the other hand, DEM simulations were used to study the effect of material properties on the packing structure of fine particles due to cohesive interparticles forces [5]. The results are analyzed in terms of porosity, mean coordination number and radial distribution function. It was demonstrated that porosity can be described as a function of the force ratio between the van der Waals force and gravity force on a particle but the relationship varies with the sliding and rolling friction coefficients.

Molecular dynamics simulations were used to investigate the structure and mechanical properties of a simple two-dimensional model of a cohesive granular material [6]. Interparticle forces were used taking into account elasticity, Coulomb friction, and a short-range attraction like the van der Waals force in powders. The microstructure of the cohesive packing under low pressure was shown to depend sensitively on the assembling procedure which is applied to the initially isolated particles of a granular gas. While a direct

R. O. Uñac (✉) · A. M. Vidales
Departamento de Física, Instituto de Física Aplicada (INFAP-CONICET), Universidad Nacional de San Luis, Ejército de los Andes 950, 5700 HHW, San Luis, Argentina
e-mail: runiac@unsl.edu.ar

Published online: 05 December 2010

compression produced a final equilibrated configuration with a similar density to that of cohesionless systems, the formation of large aggregates prior to the application of an external pressure resulted in much looser stable packings.

A physical and numerical work studying the settling of uniform spheres in liquids has shown that interparticle forces play a critical role in forming the so-called random loose packing (RLP) [7]. In the same year, three-dimensional molecular dynamics simulations were performed to study stress transmission in wet granular media in the pendular state [8]. It was shown that the tensile action of capillary bonds induces a self-stressed particle network organized in two percolating "phases" of positive and negative particle pressures. When a confining pressure was applied, the number of tensile bonds falled off and the negative phase broke into aggregates and isolated sites.

Three dimensional contact dynamics simulations of cohesive powders have been used to study porosity under weak uniaxial compression [9]. Rigid spherical particles of identical sizes were considered, but force and also torque transmission were allowed at contacts. The total normal force between two grains has two constituents: an attractive part, which is a constant cohesion force, and a force due to the excluded volume constraint. Authors found that the porosity is well represented as the sum of independent contributions of the torsion and rolling friction. Their results suggest that each relative motion mode, if it is suppressed, results in an additional free volume in the system independently of the other modes.

In the same context of contact dynamics but in two dimensions, authors in [10] have proposed a model to capture the essential microscopic physical processes underlying the dynamics of a collapsing suspension/soil. They compared the model with real data obtained from in situ measurements performed with a natural collapsing/suspension soil. They presented the consistency between the shear strength behavior of their collapsing suspension/soil model and the behavior of the real system, for both the unperturbed and the perturbed phases of the material. In their work, the bonding between two particles is considered in terms of a cohesion model with a constant attractive force acting within a finite range, so that for the opening of a contact a finite energy barrier must be overcome. In that paper the cohesion force dominates the behavior and the energy barrier plays a minor role but its existence is of crucial importance to avoid simulation artifacts. The main characteristic of the metastable granular structures investigated by them is that they collapse, e.g. when an external load is applied.

Numerical simulations have also been used to observe and characterize, at both macroscopic and microstructural levels, the consolidation behavior in isotropic compression of model cohesive powders [11]. In that paper, authors focused on the effect of geometry and collective rearrangements on the material behavior. They observed the loose packing states, as assembled under growing confining pressure, to undergo important structural changes, while the solid fraction parameter irreversibly increases. They found their results shown qualitative differences between cohesive and cohesionless granular systems. Some of the main differences are the presence of stable loose structure and the compaction phenomenon due the cohesion in the macroscopic behavior. Due to the fact that attractive and repulsive contact forces, of the order of tensile strength, tend to compensate under low pressure, the force distribution and the values of intergranular forces were not simple to estimate at the microstructural level.

It is well known that both in dry and wet granular systems, forces are transmitted only through interparticle contacts, leading to strong inhomogeneities through a system [12]. In this sense, a packing of cohesionless grains that has a given anisotropy can develop a change in its contact network due to the presence of cohesion forces, leading to the formation of different kind of contacts along preferential directions. This structural change translates into changes in macroscopic quantities such as, for instance, the compaction capacity of a system of wet grains. For this reason, some authors have referred to the anisotropy as a relevant parameter to reflect those changes [13]. In this sense, authors in [14] have investigated the bulk microstructure in cohesive powders. They were able to link the compressive strain with the measured anisotropy, thus creating the link between macroscopic and microscopic behaviours.

In [15] the probability density functions of normal forces in dry and wet granular systems from 3D simulations by molecular dynamics and contact dynamics methods have been compared. Using a model of capillary cohesion, implemented as a force law expressing the capillary force as a function of water volume and the distance between particles, it was found that force distributions were exponential for both compressive and tensile forces.

Given the state of the art, we considered it is appropriate to develop simple models to calculate some parameters to characterize the mechanical state of a granular system in the presence of moisture. In this sense, pseudodynamic simulations have proven to be useful for analyzing the packing fraction of a two dimensional bed of disks subject to tapping [16–18]. One of the important aspects to consider in such systems is the structure of the packing as a function of liquid content and the intensity of tapping.

A wet granular sample at low content of liquid has a network of capillary bridges connecting the grains. The structure of this network of bridges largely determines the mechanical properties of the sample [1,19]. We consider situations in which the cohesion is higher than other effects due to the presence of fluid in the system such as lubrication and viscosity. Our model represents a set of grains in the so-called pendular state, according to the liquid content rate [1].

In the pendular state particles are held together by attraction of capillary bridges at their contact points. In a wet sample, the capillary bridge is formed when two adjacent particles have a point of contact. At this point, the liquid surface of the films that wet the particles has a sharp bend. This in fact is not an equilibrium situation. When liquid films meet, the curvature of the liquid surface is very large and negative. This creates a major depression that sucks the liquid into the contact region. Equilibrium is reached when the liquid has acquired a spatially constant mean curvature. If the particles are moved away from each other by a certain distance, a so-called pendular bridge appears due to the bridge stretching [2].

In an earlier paper [18], we have presented a simple model to describe the response of a granular bed to a tapping-like excitation when grains can form capillary bridges due to the presence of interstitial liquid. In that paper, a pseudodynamic simulation method (PMDM) of adhesive hard disks was implemented. The PMDM method has proven to be a satisfactory tool taking into account that due to the high compactness of the system a grain never gets sufficient time to accelerate to large velocities [16,20]. In [18], the packing fraction and coordination number after the steady state of the tapping process has been reached were investigated and compared for different tapping intensities and liquid contents. We found some contrasting behavior with dry systems and qualitative agreement with experimental data.

Regarding the cohesive force used in our model and comparing it to some of the above mentioned models, we remark that our cohesion model introduces the non homogeneity of the liquid distribution between particles through a stochastic component for the force, i.e., the model has a non deterministic character for the formation of capillary bridges. This stochastic character will be described in more detail below.

Our main objective here is to complete the study of the structural properties of systems subjected to tapping as they achieve the steady state. So, we present here results on the anisotropy of wet granular media subject to tapping and on the distribution of contact angles. We will describe and show that anisotropy is not always a parameter that completely reflects the structure of packing. However, the distribution of contact angles will help us to infer the pattern of the packing structure in all situations.

2 Simulation model

The simulation method for a wet granular bed used here has been depicted in a previous work, for additional technical details and model assumptions, the reader might refer to [16–18]. For the sake of completeness, we provide a summarized description below.

The simulation model used is a pseudodynamic algorithm which allows to deposit inelastic hard disks in a rectangular container thus forming a two-dimensional packing. Differently than molecular dynamics method, the equations of motion are not solved for the interacting grains. The movement of a grain is always performed in the direction of gravity unless local geometrical constrains exerted by other particles make the falling grain to stop or rotate. Basically, the method consists in small falls and rolls of the grains until they come to rest by contacting other particles or the system boundaries. In the case of dry disks, it is consider that a disk is in a stable position if it has reached two contacts such that the x-coordinate of its center of mass lies between them.

The deposition algorithm consists in picking up a disk in the system and performing a free fall of length δ. If in the course of that fall a disk collides with another disk (or the base), the falling disk is put just in contact and this contact is defined as its first supporting contact.

If the disk has already one single supporting contact we let it rotate an arc-length δ around the point of contact with its supporting particle. Clearly, the contact point moves as the disk rolls over the other. If in the course of a roll of length δ a disk collides with another disk (or a wall), the rolling disk is put just in contact. If the first supporting contact and the second contact are such that the disk is in a stable position, the second contact is defined as the second supporting contact; otherwise, the lowest of the two contacting particles is taken as the first supporting contact of the rolling disk and the second supporting contact is left undefined. Disks with two supporting contacts are considered stable and left in their positions. A moving disk can change the stability state of other disks supported by it, therefore, this information is updated after each move. The deposition is over once each particle in the system has both supporting contacts defined or is in contact with the base (particles at the base are supported by a single contact).

Particles are moved one at a time, but they perform only small moves that do not perturb to a significant extent the ulterior motion of the other particles in the system. Particles are moved always in the same order although this order does not affect the final state of the system.

Iteration consists in moving every disk in the system by a distance δ—or the amount allowed by the constraints imposed by neighboring disks. Notice that after iteration many disks may be left in unstable positions. A number of iterations are needed before every disk finds its stable configuration. For very small values of δ, this method yields a realistic simultaneous deposition of grains with zero restitution coefficient. An important point in this simulation is the effect that the parameter δ has in the results since particles do not move simultaneously but one at a time. One might expect that in the limit $\delta \to 0$ we should recover a fairly realistic dynamics for fully inelastic rough disks dragged downwards

at constant velocity [17]. The dependence of the results on parameter δ has already been studied [17]. Since results agree within statistical uncertainties for $\delta \leq 0.01$ we decided to use this maximum value as a convenient choice for our simulations. Lower values of δ require larger CPU times; whereas for δ above 0.01, the results depend on δ.

This model has been deeply described elsewhere and we will avoid extending too much the explanation here. We remit the interested reader to references [16,17].

Within this model, one may introduce cohesive forces due to capillary liquid bridges formed by the presence of moisture in the system. A wet granular sample at low content of liquid presents a network of capillary bridges connecting the grains. The structure of this network of bridges determines to a large extent the mechanical properties of the sample [1,19]. We consider situations where cohesion outweighs other effects of the presence of liquid in the system such as lubrication and viscosity. Our model represents a granular assembly in the so called "pendular state" according to the classification by liquid content [1]. In the pendular state particles are held together by the attraction of the capillary bridges at their contact points.

In a wet sample, capillary bridges form when two adjacent particles have a contact point. If the particles are moved away from each other by a certain distance, a so-called pendular bridge appears due to the bridge stretching [2].

Taking into account the four main factors affecting the total capillary force in a static liquid bridge [21], we assume that: the first factor, the wetting angle, is zero (complete wet); the second one, the surface tension of the liquid, is constant all over the system; the remaining factors, (the separation distance between two particles and the liquid bridge volume), can be considered as stochastic variables since each bridge in the system may have a different volume and separation depending on local conditions and contact history [18]. We introduce these two important factors through a single parameter P_0 that will be described below. It is important to notice that in the above mentioned pendular state some particles may be stable thanks to the geometrical constrains imposed by others. In this situation capillary bridges may exist at the contact points with the supporting grains; however, the stability of the particle is not determined by these bridges. In our model we will only count as a capillary bridge the particle–particle contacts that support the entire weight of one of the touching grains.

In Fig. 1, we show a scheme of the balance of forces on a given particle i of weight W that is in contact with a lower partner j. Assuming the suction $F_{\rm suc}$ [1] does not depend on the angle γ between two particles, the forces involved will be

$$\vec{F}_n = \vec{F}_{\rm suc} + \vec{W}_n = (F_{\rm suc} + W\sin(\gamma))\,\vec{n} \quad \text{in the normal direction} \tag{1}$$

$$\vec{F}_t = W\cos(\gamma)\vec{t} \quad \text{in the tangential direction} \tag{2}$$

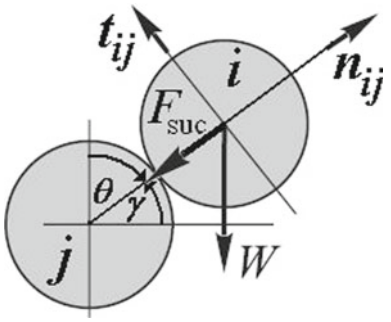

Fig. 1 Schematic diagram of forces acting on a particle i that forms a capillary bridge after contacting another grain j during deposition. W is the weight of particle i and $F_{\rm suc}$ is the average suction force

On the one hand, provided that particle j is fixed in its position, the normal force F_n is responsible for the adhesion of particle i onto the bottom partner j. On the other hand, the tangential force $F_{\rm t}$ provides the torque that drives particle i into rolling on top of particle j. Let us assume that the average suction is x times the weight of a particle (i.e. $F_{\rm suc} = xW$). We consider monodisperse systems where all particles have the same weight. Then, we have $F_n = W[x + \sin(\gamma)]$. This means that the total force that is responsible for maintaining the particles in contact will vary between $W(x+1)$ and $W(x-1)$ as γ goes from $\pi/2$ to $-\pi/2$. For $x < 1$, negative values of F_n are obtained for some configurations of dangling disks ($-\pi/2 < \gamma < 0$). This corresponds to the normal component of the particle weight overcoming the suction, which invariably leads to the detachment of the dangling disk.

We represent capillary bridges through a stochastic mechanism so that a particle may be stuck during its rolling down over another particle due to suction. The actual sticky probability $P_{\rm sticky}$ is then proportional to the normal force applied on the rolling particle at a given angle γ measured from the horizontal [18]. Thus, it is given by:

$$P_{\rm sticky}(\gamma) = \max\left\{0,\, P_0\frac{[x+\sin(\gamma)]}{x+1}\right\} \tag{3}$$

The normal force has been divided by its maximum possible value in this equation. We have also introduced the proportionality constant P_0 to control the maximum sticky probability. For $P_0 = 1$ the stickiness is maximum whereas for $P_0 = 0$ particles do not stick, which corresponds to the dry case. In this way, we can test different overall sticky probabilities emulating a variation in liquid content within the pendular state.

The max function in Eq. (3) takes care of the situation where $x < 1$ for which the second argument may become negative indicating that the particle must detach (i.e., $P_{\rm sticky}(\gamma) = 0$). Nevertheless, all our simulations have been carried out setting $x = 1$.

As explained in [18], the pseudodynamics for the sticky disks is carried out in much the same fashion as for hard disks

[17]. Following the steps for the simulation process already depicted in detail in that paper, we will just recall here some of the main features necessary for understanding the results presented and discussed in the present paper.

If in a given iteration a disk already has one single potential supporting contact there are two possibilities: (1) to stick through a capillary bridge to the supporting particle and so become immobilized (probability $P_{\text{sticky}}(\gamma)$), or (2) to move on by either a roll or a free fall. A particle that sticks is an example of the situation in which the strength of the capillary bridge is enough to prevent the particle from further rolling on top of its supporting disk. If the supporting particle does not move further in future time steps the disk will remain in its stable position held by the capillary bridge.

A particle that does not stick to its first potential support (probability $[1 - P_{\text{sticky}}(\gamma)]$) corresponds to the situation in which either a capillary bridge does not form at the contact or the weight of the disk overcomes the strength of the capillary bridge. For this reason the particle can roll down the surface of the lower partner. If a bridge exists, and the suction is not too weak, one expects that the particle may keep rolling without detaching from the surface of the contacting disk even after reaching a lower position with respect to its partner. All along the rolling the disk has a chance to stick $[P_{\text{sticky}}(\gamma)]$ at every iteration and become immobilized. However, once the particle has rolled to a position beneath its supporting partner, and provided that the particle does not stick, there is a probability for the particle to detach and fall freely and a probability for it to keep rolling in contact. We use again $P_{\text{sticky}}(\gamma)$ to set the probability that a particle dangling beneath its support will roll in contact without detaching. This probability does not need to be the same as the sticky probability, but it has to be related to the strength of the capillary bridge. We have chosen $P_{\text{sticky}}(\gamma)$ for this probability to reduce the number of control parameters in the model. Notice that in this case the disk is not stuck—i.e., it is not immobilized—but remains in contact. In the next iteration, the disk will again have the chance to stick. It is worth mentioning that, since in our simulations $P_{\text{sticky}}(-\pi/2) = 0$ (recall that $x = 1$), all particles that do not stick but roll dangling from its partner will eventually detach at the point $\theta = -\pi/2$, unless a second contact is formed during rolling.

In summary, a particle that contacts another disk with $0 < \gamma < \pi/2$ has a probability $P_{\text{sticky}}(\gamma)$ to stick and a probability $[1 - P_{\text{sticky}}(\gamma)]$ to roll. However, if $-\pi/2 < \gamma < 0$, the particle has a probability $P_{\text{sticky}}(\gamma)$ to stick, a probability $[1 - P_{\text{sticky}}(\gamma)]P_{\text{sticky}}(\gamma)$ to roll, and probability $[1 - P_{\text{sticky}}(\gamma)]^2$ to detach.

After the array of particles attains a stable configuration, a tapping process is started. All vertical coordinates are multiplied by a factor $A > 1$ and the particles are also allowed to move under random displacements of length $0 < \xi < A - 1$ [18]. As frequently used, we employ $\Gamma = \sqrt{A - 1}$ as a measure of the tapping intensity. This quantity is proportional to the energy input given by a realistic tap with peak acceleration Γg, with g the acceleration of gravity [22].

3 Previous results and anisotropy calculation

Based on the simple model for wetting grains described above, a study on the response of a granular bed subjected to a tapping-like excitation was presented in a previous work [18]. In that paper, results of the behavior of the mean packing fraction, $<\phi>$, and mean coordination number, $<z>$, after the steady state of the tapping process has been reached, are compared for different tapping intensities and liquid contents. Extensive simulations were performed with a rectangular box of width $L = 20$ where 1,000 monosized disks of radius $r = 0.1 + 1/\sqrt{2} \approx 0.807$ were deposited. The number of particles used in our simulations is the minimum necessary to save computing time without significant size effects.

We have chosen the parameter x that accounts for the strength of the suction in such way that a particle dangling right beneath another disk has probability 1 of falling freely, i.e. $x = 1$. This situation corresponds to the case where the suction is just as strong as the weight of the particle.

In Figs. 2 and 3 we show the corresponding behavior found for $<\phi>$ as a function of tapping intensity Γ and liquid content P_0. These results show that the increase of P_0 promotes the formation of open chain like structures with very low packing fractions (below 0.5 at high tapping intensities) and low coordination numbers. However, the effect of the increase of P_0 levels off beyond $P_0 = 0.125$. At low tapping intensities it is possible to reach relatively high packing fractions even with large liquid contents.

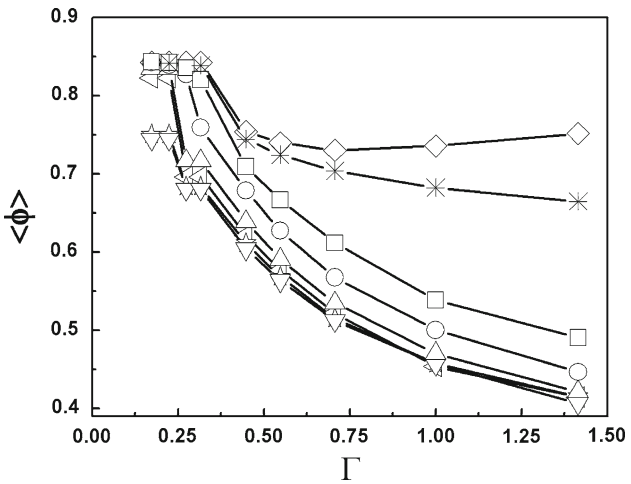

Fig. 2 Mean steady state packing fraction $<\phi>$ as a function of tapping intensity Γ at different liquid content (as measured by the sticky probability P_0). From top to bottom $P_0 = 0.0, 0.005, 0.025, 0.05, 0.125, 0.25, 0.5, 1.0$ (see Ref. [18])

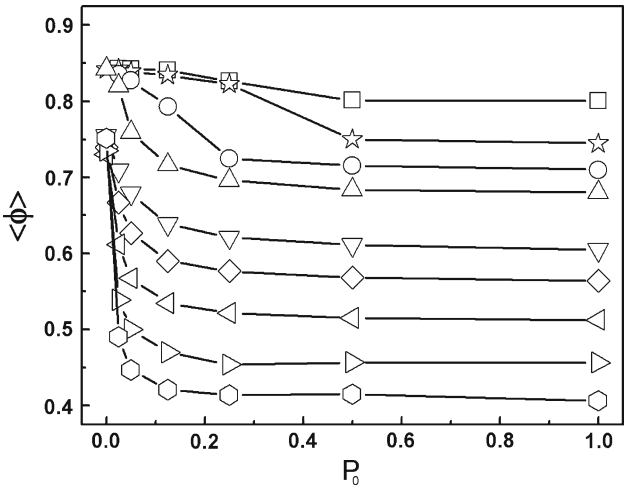

Fig. 3 Packing fraction $<\phi>$ as a function of liquid content P_0. Each curve corresponds to a different tapping intensity as follows: $\Gamma = 0.173$ (*squares*), 0.224 (*stars*), 0.274 (*circles*), 0.316 (*up triangles*), 0.448 (*down triangles*), 0.548 (*diamonds*), 0.707 (*left triangles*), 1.000 (*right triangles*), 1.414 (*hexagons*) (see ref. [18])

In this context, it is interesting to analyze the structure of the resulting packings in the course of tapping in terms of the anisotropy. In [18] it was found that even in the dilute case, the structure keeps a signature of a triangular lattice with contact normals along particular directions. In this sense, the key questions would be how does the anisotropy evolve with the number of taps and how does it depend on the parameters Γ and P_0.

The evolution of the packing structure will depend on the rearrangements of the relaxation process, thus, the extent of the tapping intensity and the probability for the formation of capillary bridges will control the directional ordering of the contact network. Typically, the distribution of contact directions can be characterized by means of the fabric tensor $\boldsymbol{F}$ defined by the following equation [13,23]:

$$F_{\alpha\beta} = \frac{1}{N}\sum_{i=1}^{N} n_\alpha^i n_\beta^i \tag{4}$$

where N is the total number of contacts in the packing, $\mathbf{n}^i$ is the normal contact vector whose components are $\sin\theta^i$ and $\cos\theta^i$, while n_α^i and n_β^i are, respectively, the α and β components of $\mathbf{n}^i$. Figure 1 shows a schematic representation of a contact formed by a falling particle i with particle j in the array. The contact between the two particles is represented by the segment joining the two centers of the them. The angle θ^i of this contact is indicated respect to the vertical direction and coincides with the direction of the normal contact.

The fabric tensor can be calculated when the distribution of contact directions is measured. Once the tensor is constructed, its eigenvalues f_1 and f_2 can be determined and the structural anisotropy characterizing the packing is computed from:

$$a = 2(f_1 - f_2) \tag{5}$$

In the next section we will discuss the results obtained by the computation of a on the packings generated for different values of Γ and P_0 already shown in Figs. 2 and 3.

4 Results and discussion

Figure 4 shows the results obtained when anisotropy a is calculated on the final structure of a packing after 1,500 tappings at a given intensity Γ. Each curve represents the behaviour for a different liquid content P_0. Comparing this plot with that of Fig. 2, we see that for $\Gamma \geq 0.447$, systems with lower liquid content (which present a higher degree of compaction)

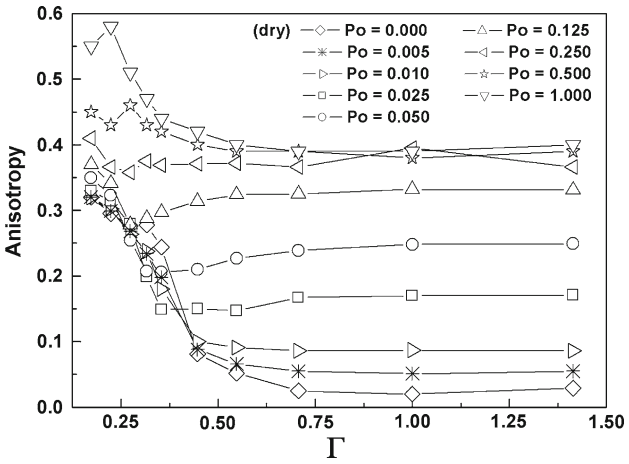

Fig. 4 Anisotropy as a function of tapping intensity at different liquid content. For $P_0 = 0.0$ (*dry case*) and from $P_0 = 0.005$ to $P_0 = 1.0$ (*wet cases*)

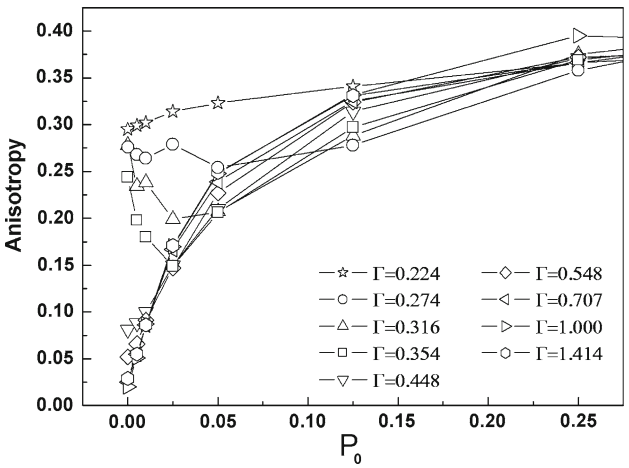

Fig. 5 Anisotropy as a function of liquid content P_0. Each curve corresponds to a different tapping intensity from $\Gamma = 0.224$ to $\Gamma = 1.414$

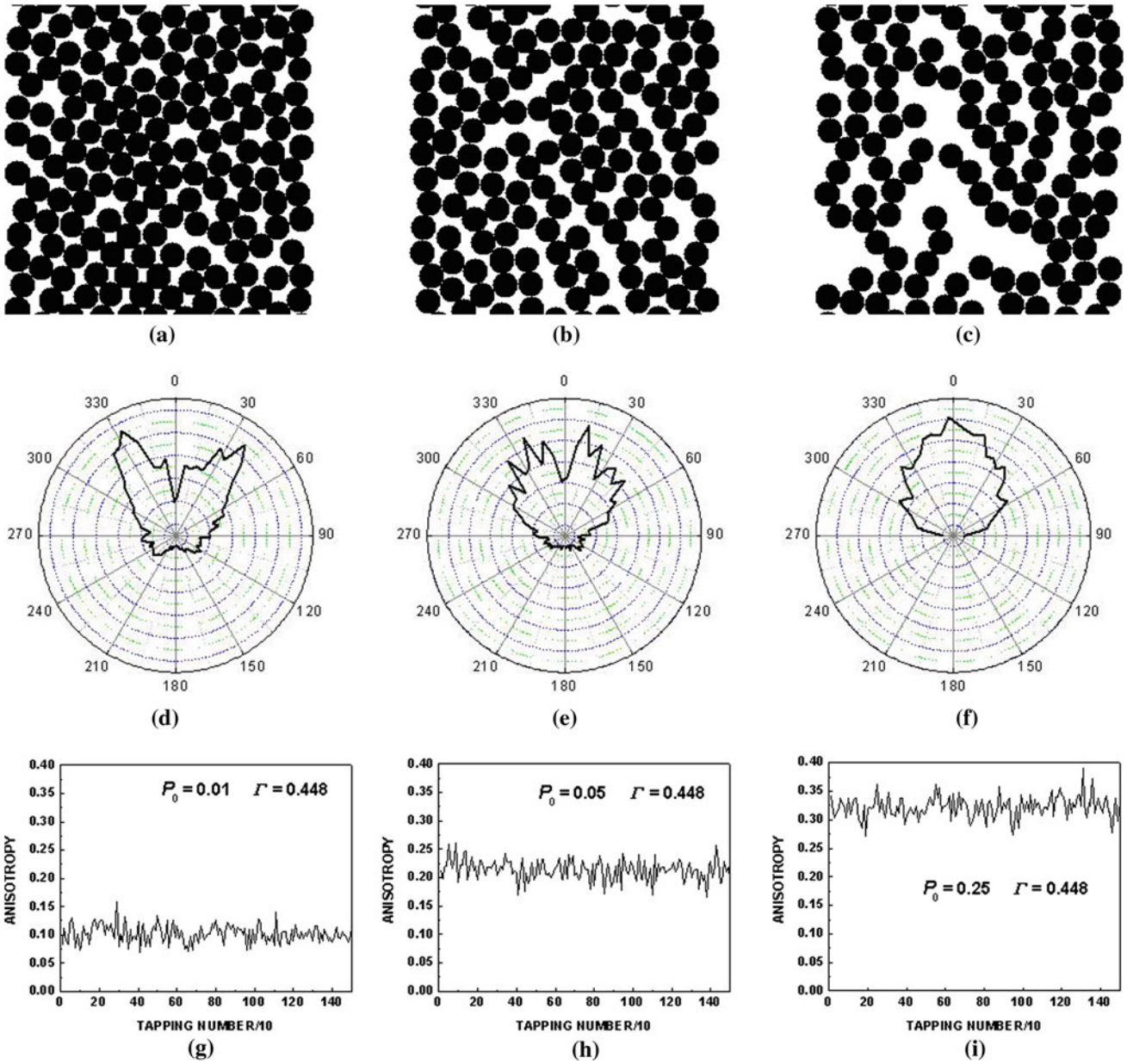

Fig. 6 *First row*: snapshots of a fully deposited bed of disks after 1,500 taps for $P_0 = 0.01$ (**a**), 0.05 (**b**), 0.25 (**c**). All systems were tapped at $\Gamma = 0.448$. Only part of the whole assembly is shown. *Second row*: (**d–f**) polar diagrams of the distribution of contact angles for packings in the first row, respectively. *Third row*: (**g–i**) anisotropy as a function of tapping number for the same packings, respectively

have the lowest values of anisotropy. In this region and for a given P_0, a shows almost constant values as Γ increases. However, for $\Gamma < 0.447$, curves show interesting features that can be analyzed better if we plot the anisotropy in terms of P_0. For this reason, we present the behavior of a vs. liquid content at different tapping intensities in Fig. 5. Keeping in mind the results for $<\phi>$ vs. P_0 presented in Fig. 3, one could say that, while packing fraction decreases with P_0, anisotropy has an increasing trend. Non monotonic behavior of a for certain values of Γ leads us to analyze in greater detail the results shown in Fig. 5, where three different families of curves can be distinguished: (i) for $\Gamma \geq 0.447$, (ii) for $0.274 < \Gamma \leq 0.354$ and (iii) for $\Gamma \leq 0.274$.

For case (i), we note that a increases monotonically with increasing P_0. Anisotropy tends to zero when liquid content also tends to zero (dry limiting case).

In Fig. 6 (parts a–c), we display a set of snapshots for the typical change in the structures of the packings as P_0 increases from 0.01 to 0.25 with a tapping intensity $\Gamma = 0.447$. In the same figure, the second row shows the polar diagrams of the distribution of contact angles corresponding the the same packings (parts d–f). The last row of Fig. 6 plots

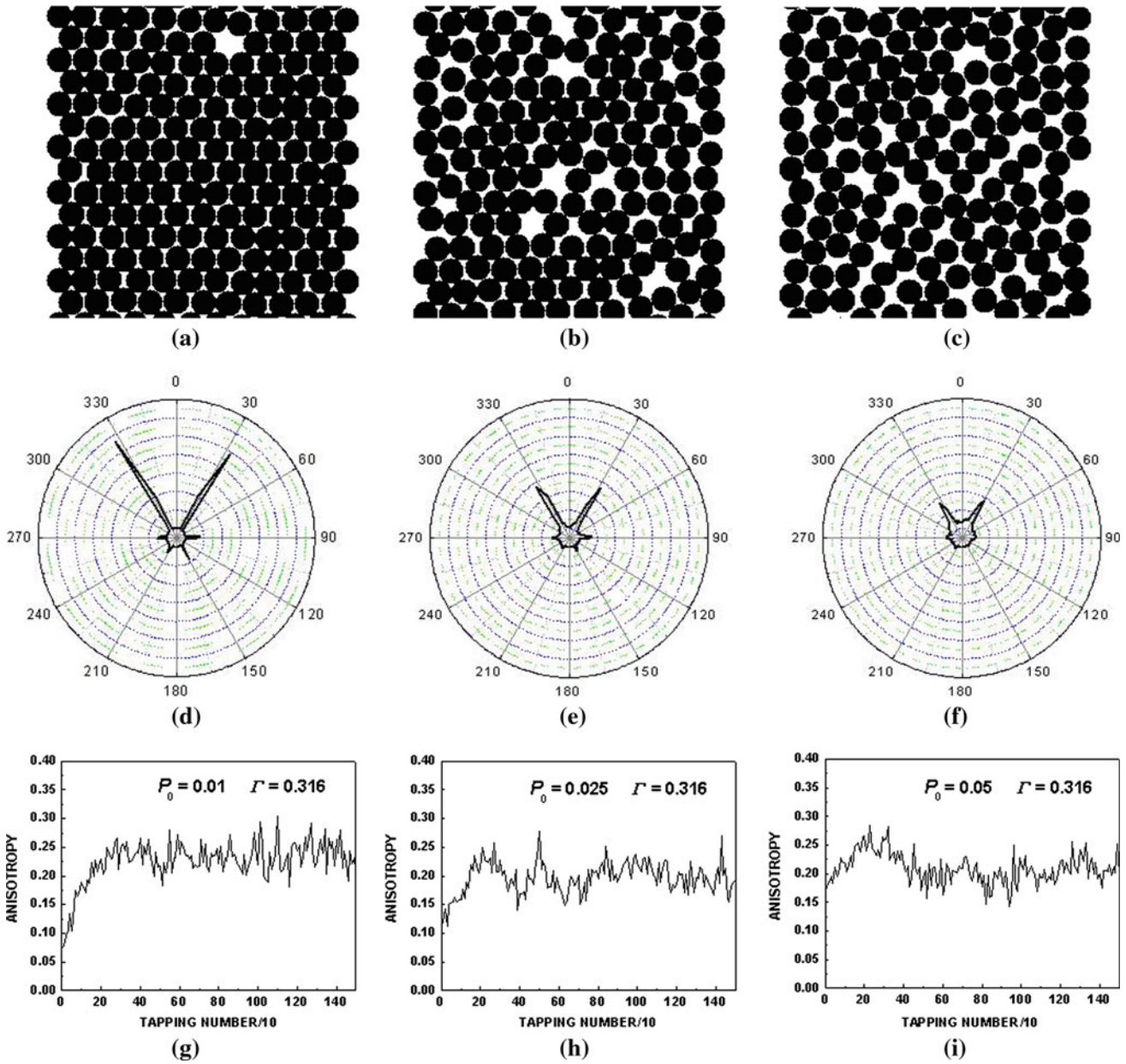

Fig. 7 *First row*: snapshots of a fully deposited bed of disks after 1,500 taps for $P_0 = 0.01$ (**a**), 0.025 (**b**), 0.05 (**c**). All systems were tapped at $\Gamma = 0.316$. Only part of the whole assembly is shown. *Second row*: (**d**–**f**) polar diagrams of the distribution of contact angles for packings in the first row, respectively. *Third row*: (**g**–**i**) anisotropy as a function of tapping number for the same packings, respectively. The scale for the polar plot is 7 times smaller than the corresponding for the preceding figure to highlight the different features

the evolution of a as a function of the number of tappings (parts g–i).

Looking at Fig. 6a (low liquid content), a disordered structure can be observed. The angular distribution of contacts (Fig. 6d) indicates that there are two moderately preferred orientations around directions 30° and 330°, with a low intensity at 0°, keeping a typical signature of a triangular lattice. In addition, there is a not so even distribution with low intensity for contacts angles greater than 90° and smaller than 270°, representing the directions of capillary bridges exclusively. The corresponding evolution of a with tapping number shows that only fluctuations around a constant value are possible (Fig. 6g).

Figure 6b (moderate liquid content) shows a more chain-like structure for particles, resulting in a more open structure compared with the previous case. The preferential orientation of these chains is depicted by the polar distribution in Fig. 6e. The contacts are distributed with greater uniformity,

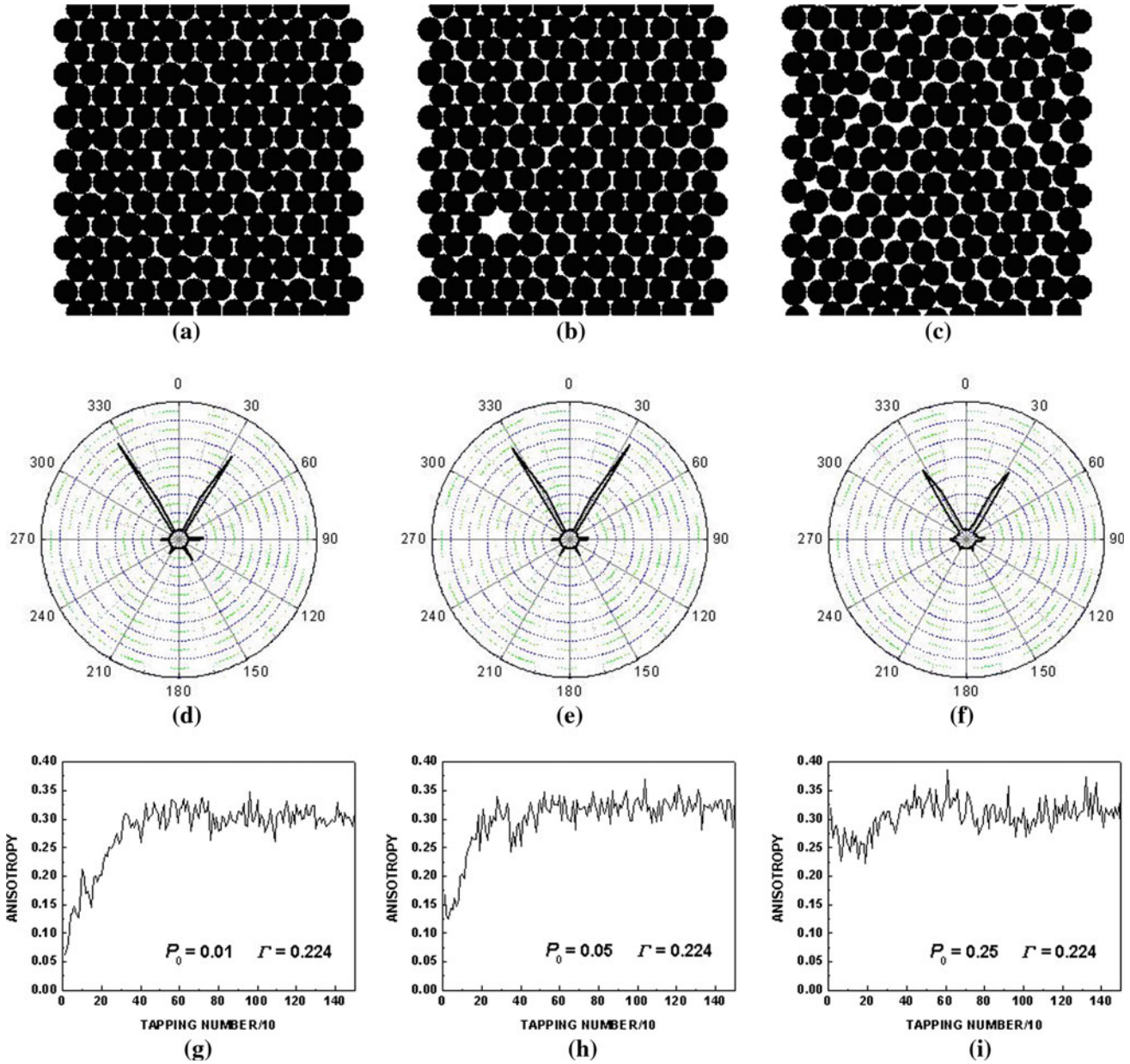

Fig. 8 *First row*: snapshots of a fully deposited bed of disks after 1,500 taps for $P_0 = 0.01$ (**a**), 0.05 (**b**), 0.25 (**c**). All systems were tapped at $\Gamma = 0.224$. Only part of the whole assembly is shown. *Second row*: (**d**–**f**) polar diagrams of the distribution of contact angles for packings in the first row, respectively. *Third row*: (**g**–**i**) anisotropy as a function of tapping number for the same packings, respectively. The scale for the polar plot is 7 times smaller than the corresponding for Fig. 6 to highlight the different features

i.e., the trace of a triangular distribution of contacts is less visible. Several peaks at different orientations appear for angles greater then 60° and smaller that 300°. Besides, the number of contacts oriented at 0° increases. Anisotropy is greater than for the case before, with fluctuations around a constant value.

Figure 6c (high liquid content) shows an even more chain-like structure compared with the two previous cases. The chains of particles are mainly oriented in an almost vertical direction. The angular distribution of contacts has a maximum at 0° and is fairly evenly distributed between 60° and 330°. Practically, there are no contacts for angles between 90° and 270° which correspond to contacts associated with capillary bridges exclusively. Here again, anisotropy shows fluctuations around a constant value that is greater than for precedent cases.

In short, the increment of P_0 results in an increment in the chain-like structure of the packing. The angular distribution

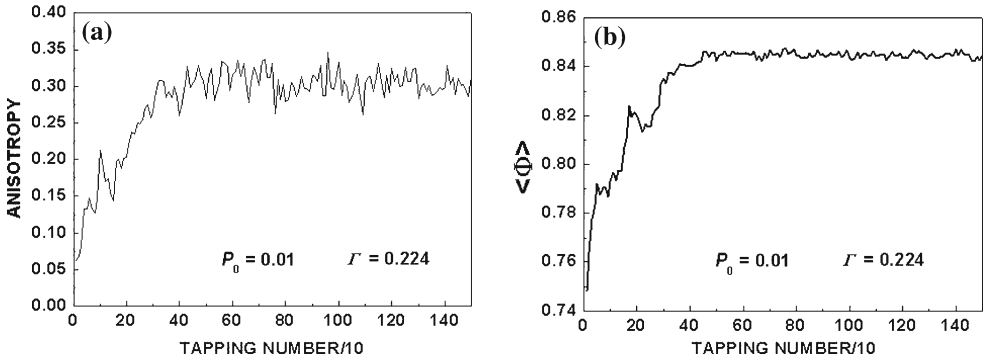

Fig. 9 Comparison between the behavior of packing fraction and anisotropy as a function of the tapping number for the case $\Gamma = 0.224$ and $P_0 = 0.01$

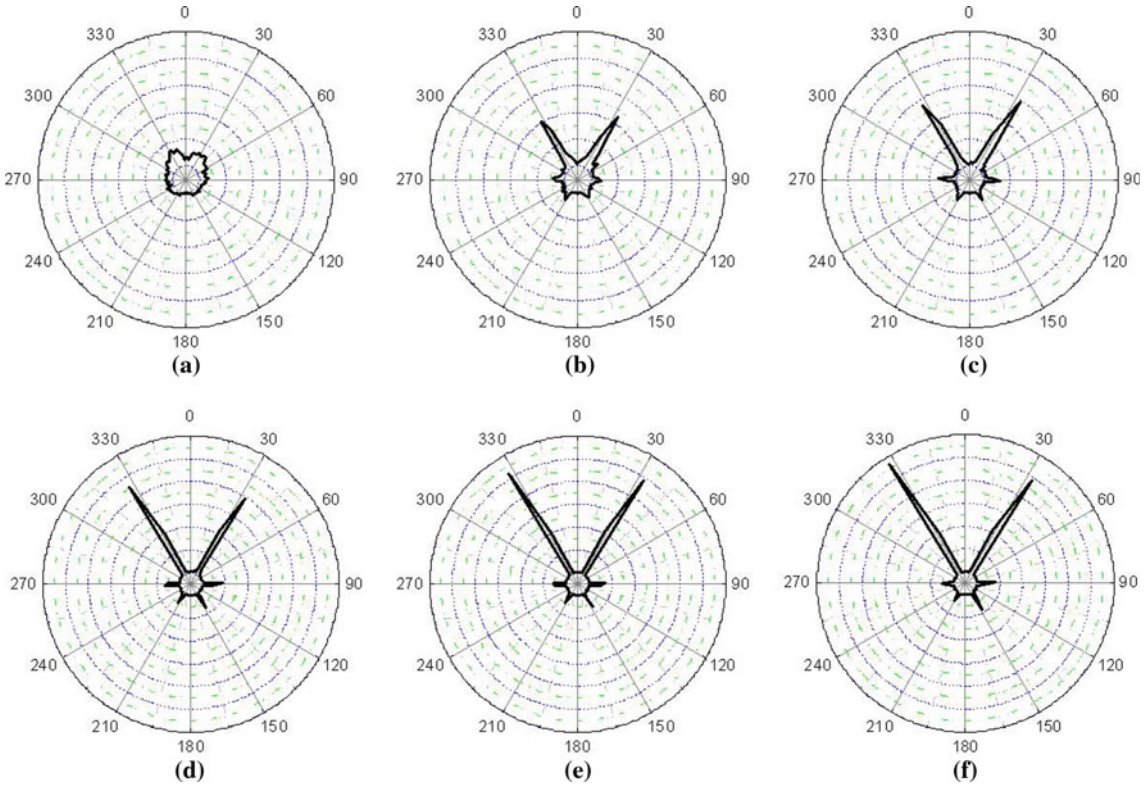

Fig. 10 Evolution of polar diagrams of the distribution of contact angles at different tapping number: 1 (**a**), 100 (**b**), 200 (**c**), 300 (**d**), 450 (**e**) and 600 (**f**)

of the contacts changes from a disordered structure that keeps a poor signature of a triangular lattice to a nearly vertical chain configuration. Anisotropy increments are related to this preferential orientation of chains that show up as a result of a high probability for the formation of capillary bridges (Eq. 3). This behavior explains the fact that, at this extent of tapping intensities, the packing fraction decreases, as was reported in [18].

Concerning the changes of a with the number of tappings, the trends observed in the three plots follow the same qualitative behavior found for the corresponding packing fraction results. We will show some examples later on.

As can be appreciated in Fig. 5, the curves belonging to case (ii) present, for low liquid content, a decrease of a with P_0 until they find the value of anisotropy corresponding to case (i). From then on, anisotropy starts to rise following the set of curves of case (i).

Figure 7 (parts a–c) shows that the structure, initially ordered in a rather triangular pattern, starts to disorder as P_0 grows. This is reflected by the probability distribution of

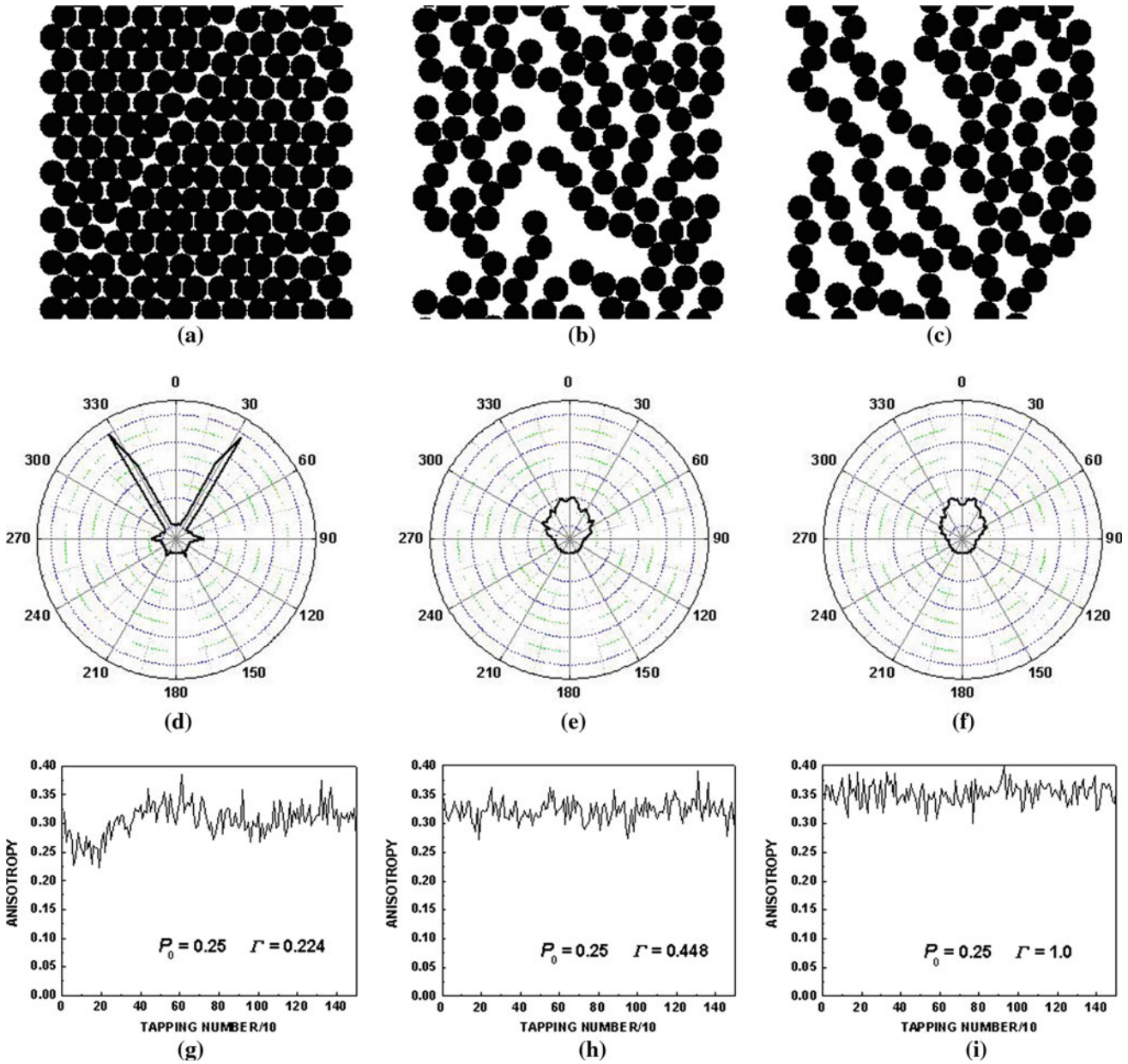

Fig. 11 *First row*: snapshots of a fully deposited bed of disks after 1,500 taps for $\Gamma = 0.224$ (**a**), 0.448 (**b**), 1.0 (**c**). In all systems the liquid content is $P_0 = 0.25$. Only part of the whole assembly is shown. *Second row*: (**d**–**f**) polar diagrams of the distribution of contact angles for packings in the first row, respectively. *Third row*: (**g**–**i**) anisotropy as a function of tapping number for the same packings, respectively

angles for the contacts, shown in parts e to g in the same figure. Indeed, at low P_0, the contacts are preferentially oriented at 30° and 330° directions, which correspond to a highly triangular lattice structure. As P_0 increases, the emergence of new capillary bridges starts to distort the strong triangular trace. The peaks in the polar plots are less important and the dispersion around the preferential directions becomes evident. This translates in a change of a, showing a minimum value for certain liquid content. This behavior can be explained as the competition between two effects. At low P_0, the organization of the structure follows the steric constraints that conduct to a triangular lattice. As P_0 increases, the apparition of capillary bridges sticking the particles creates contacts in other directions close around the originals, decreasing anisotropy. As P_0 is still greater, this last effect dominates and particles start to orientate their contacts around the vertical, resulting in an increasing anisotropy. This competition effect is more evident for greater tapping

intensities. The probability for the formation of a contact (due to a capillary bridge) at a different angle than the one for a triangular structure is greater as greater is the space between particles.

For case (iii) and looking at Fig. 5, we found that a do not vary too much as P_0 increases for beds tapped at low Γ. Let us see how the packings behave for three typical points on the curve for $\Gamma = 0.224$, for example. In Fig. 8 (parts a–c) the snapshots demonstrate that the structures keep practically unchanged as liquid content increases, showing an ordered organization with a high triangular trace. This feature is reflected in the polar plots (parts d–f) that have two important peaks at 30° and 330°, and low intensity ones at 90°, 150°, 210° and 270° directions. These last four directions represent the contribution of suspended particles due to capillary bridges. Some interesting remarks show up when we analyze the evolution of the peaks as liquid content increases. For low or relatively low P_0, the probability distribution of angles is almost the same, while for greater liquid content, the contacts belonging to suspended particles tend to disappear and a little dispersion around 30° and 330° directions is observed. As a result, a small increment in a is obtained for this last case.

It is worthy to mention that in all the cases above the changes of a with tapping number qualitatively mirror the behavior of the packing fraction. For the sake of brevity, we will show just one plot for $\Gamma = 0.224$ and $P_0 = 0.01$. Figure 9 displays the comparison. It is clear that for this case the packing fraction growth is accompanied by an increase in anisotropy. This increase in a is due to the preferential orientation of contacts in directions corresponding to a triangular lattice. The evolution of the polar distribution of contacts vs. tapping number is plotted in Fig. 10. At the beginning, contacts are fairly distributed in upward directions with a slight preference at 30° and 330°. As the tapping process is in progress, growth of the peaks in those directions is evident.

At this stage, it is interesting to go back to Fig. 5. Close around $P_0 = 0.25$, anisotropy for all tapping intensities does not change too much. However, packing fraction is greater at lower tapping intensities (see Fig. 3). To clarify this point, Fig. 11 shows the polar graphs and snapshots for $P_0 = 0.25$ and three different values of Γ. It is clear that the arrangement of particles is very different as Γ increases. The polar graphs show the different distribution of contacts for each case. For small Γ, structure retains the triangular appearance. As Γ increases and more space is available for particles to establish capillary bridges in different directions during the relaxation process (after each tapping), contacts between particles can reorient losing the trace of the triangular array and forming chains around the vertical direction. This results in the reduction of the compaction capacity associated with more open structures. At this point, we should note that the distribution

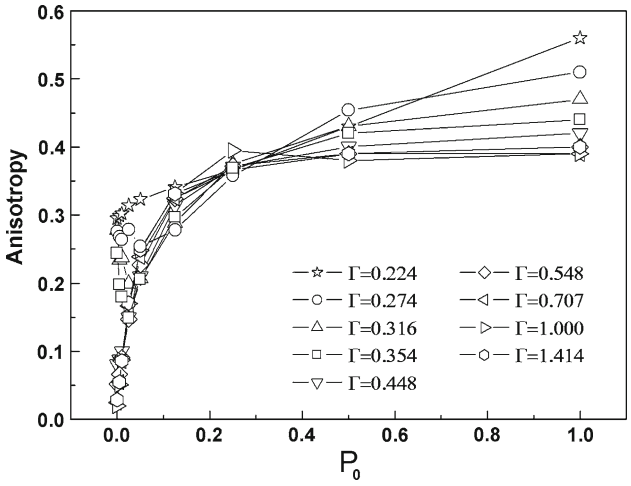

Fig. 12 Anisotropy as a function of liquid content for all the range of P_0. Each curve corresponds to a different tapping intensity as in Fig. 5

of angles well describes the topological properties of the system in all cases.

Going further in the analysis, Fig. 12 presents the behavior of a for all the range of P_0. For $0.5 < P_0 \leq 1$ anisotropy clearly depends on tapping intensity. In Fig. 13 we show the results for $P_0 = 1.0$ and three different values for Γ. Here again the corresponding distributions of contacts are different for each case. At low Γ (part a) the particles conform nearly vertical chains. On the other hand, as the tapping intensity is higher (parts b and c) the chains branch. The polar plots reflect this behavior. The contact distribution shows a clear preferential orientation at 0° for low Γ (part d), whereas for higher Γ (parts e and f) contacts are distributed over a range between 60° and 300°.

The analysis of the last two paragraph shows that for low Γ the effect of liquid content is determinant in the final structure adopted by the particles. The preferential directions change substantially with P_0 (compare Fig. 11a with Fig. 13a), resulting in an increased anisotropy. However no large differences were found for the other two intensities, although there is an increase of contacts in the vertical direction for $P_0 = 1$ compared with $P_0 = 0.25$. The precedent discussion again demonstrates that a alone is not a good quantitative indicator to analyze the compaction capacity of a system.

It is important to mention that the results obtained here for a at $P_0 = 1$ and low Γ approaches the value calculated for a random ballistic deposition model controlled by a critical angle [13]. The value calculated here ($a = 0.58$) is lower than the theoretical value of 2/3 calculated for that model because in [13] sticking of the particles have a deterministic character that only depends on the critical angle, while here it is conducted stochastically (Eq. 3).

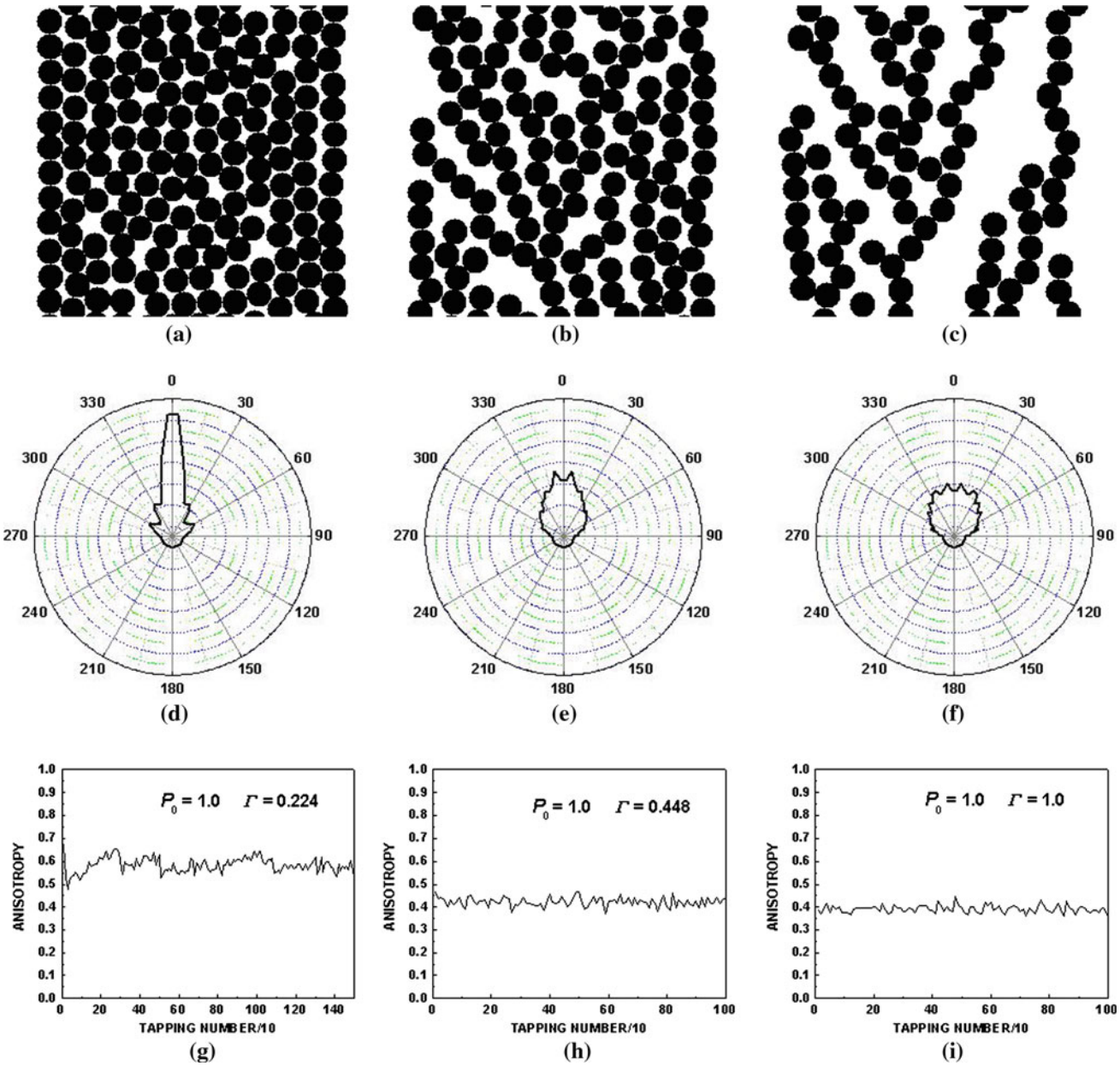

Fig. 13 *First row*: snapshots of a fully deposited bed of disks after 1500 taps for $\Gamma = 0.224$ (**a**), 0.448 (**b**), 1.0 (**c**). In all systems the liquid content is $P_0 = 1.0$. Only part of the whole assembly is shown. *Second row*: (**d**–**f**) polar diagrams of the distribution of contact angles for packings in the first row, respectively. *Third row*: (**g**–**i**) anisotropy as a function of tapping number for the same packings, respectively

5 Conclusions

Based on the results discussed so far we can conclude with some remarks on the general trends for the behavior of anisotropy observed here. From Figs. 3 and 12, as P_0 decreases, packing fraction increases while anisotropy decreases (for all Γ, in general). It should be noted that $<\phi>$ decreases monotonically with P_0 while a presents a minimum value for $\Gamma < 0.448$, except for the case of $\Gamma = 0.224$.

Looking at Figs. 2 and 4, as Γ decreases, both packing fraction and anisotropy increase, for all P_0. This is consistent with the fact that the packing keeps the almost triangular (for low and intermediate P_0) or vertically branched lattice structure (for high P_0).

In summary, there is a competition between two phenomena. On the one hand the increase in tapping intensity (introducing more void space between particles) promotes the distribution of contacts in all directions, lowering anisotropy. On the other hand, a higher P_0 increases the likelihood

of "freezing" contacts in certain directions, favoring the emergence of privileged orientations in the capillary bridges. This produces a freeze on the packing structure and depending on how the system reaches equilibrium, anisotropy will increase or decrease.

In other words, the anisotropy of the system will depend on the extent of tappings introducing disorder competing with the potential freezing of this disorder given by the value of P_0. This explains the non monotonic behavior shown in Fig. 12.

The above results demonstrate that anisotropy alone is not a good parameter to characterize the structure of a packing uniquely. Instead, we have shown that the distribution of contact angles allows to infer adequately the structure of the packing in all situations.

Finally, and concerning the evolution with the tapping number, anisotropy follows the same qualitative behavior than packing fraction. In general, one can expect that for $P_0 \geq 0.25$, a fluctuates around a constant value for all Γ and the same behavior is found for $\Gamma > 0.448$ and all P_0. Instead, for $\Gamma < 0.448$ and $P_0 < 0.25$, a increases with tapping number until fluctuations around a constant value show up.

The results obtained so far for the structural properties of wet particles subjected to tapping encourage us to address in the future jamming problems due to arching (for instance, during the discharge of particles in a hopper) and their relationship with those structural properties of the system.

Acknowledgments The authors thanks Dr. Luis Pugnaloni (IFLYSIB-CONICET, Argentina) for his contribution to the development of part of the code used here. Authors acknowledge financial support from CONICET (Argentina).

References

1. Mitarai, N., Nori, F.: Wet granular materials. Adv. Phys. **55**, 1–45 (2006); and references therein
2. Herminghaus, S.: Dynamics of wet granular matter. Adv. Phys. **54**, 221–244 (2005)
3. Feng, C.L., Yu, A.B.: Effect of liquid addition on the packing of mono-sized coarse spheres. Powder Tech. **99**, 22–28 (1998)
4. Zou, R.P., Xu, J.Q., Feng, C.L., Yu, A.B., Johnston, S., Standish, N.: Packing of multi-sized mixtures of wet coarse spheres. Powder Tech. **130**, 77–83 (2003)
5. Yang, R.Y., Zou, R.P., Yu, A.B.: Effect of material properties on the packing of fine particles. J. Appl. Phys. **94**, 3025–3034 (2003)
6. Gilabert, F.A., Roux, J.-N., Castellanos, A.: Computer simulation of model cohesive powders: influence of assembling procedure and contact laws on low consolidation states. Phys. Rev. E **75**, 011303 (2007)
7. Dong, K.J., Yang, R.Y., Zou, R.P., Yu, A.B.: Role of interparticle forces in the formation of random loose packing. Phys. Rev. Lett. **96**, 145505 (2006)
8. Richefeu, V., Radjaï, F., El Youssoufi, M.S.: Stress transmission in wet granular materials. Eur. Phys. J. E **21**, 359–369 (2006)
9. Bartels, G., Unger, T., Kadau, D., Wolf, D.E, Kertesz, J.: The effect of contact torques on porosity of cohesive powders. Granul. Matter **7**, 139–143 (2005)
10. Kadau, D., Andrade, J.S. Jr., Herrmann, H.J.: Collapsing granular suspensions. Eur. Phys. J. E **30**, 275–281 (2009)
11. Gilabert, F.A., Roux, J.-N., Castellanos, A.: Computer simulation of model cohesive powders: plastic consolidation, structural changes, and elasticity under isotropic loads. Phys. Rev. E **78**, 031305 (2008)
12. Radjai, F., Wolf, D.E., Moreau, M.J., Moreau, J.J.: Bimodal character of stress transmission in granular packings. Phys. Rev. Lett. **80**, 61–64 (1998); and references therein
13. Bratberg, I., Radjai, F., Hansen, A.: Dynamic rearrangements and packing regimes in randomly deposited two-dimensional granular beds. Phys. Rev. E **66**, 031303 (2002)
14. Andersson, R., Bouwman, W.G., Plomp, J., Mulder, F.M., Schimmel, H.G., De Schepper, I.M.: Structure, anisotropy and fractals in compressed cohesive powders. Powder Tech. **189**, 6–13 (2009)
15. Richefeu, V., El Youssoufi, M.S., Azéma, E., Radjaï, F.: Force transmission in dry and wet granular media. Powder Tech. **190**, 258–263 (2009)
16. Manna, S.S., Khakhar, D.V.: Internal avalanches in a granular medium. Phys. Rev. E **58**, R6935–R6939 (1998)
17. Pugnaloni, L.A., Valluzzi, M.G., Valluzzi, L.G.: Arching in tapped deposit of hard disks. Phys. Rev. E **73**, 051302 (2006)
18. Uñac, R.O., Vidales, A.M., Pugnaloni, L.A.: Simple model for wet granular beds subjected to tapping. Granul. Matter **11**, 371–378 (2009)
19. Fournier, Z., Geromichalos, D., Herminghaus, S., Kohonen, M.M., Mugele, F., Scheel, M., Schulz, M., Schulz, B., Schier, Ch., Seemann, R., Skudelny, A.: Mechanical properties of wet granular materials. J. Phys. Condens. Matter **17**, S477–S502 (2005)
20. Manna, S.S., Herrmann, H.J.: Intermittent granular flow and clogging with internal avalanches. Eur. Phys. J. E **1**, 341–344 (2000)
21. Yang, S.C., Hsiau, S.S.: The simulation of powders with liquid bridges in a 2D vibrated bed. Chem. Eng. Sci. **56**, 6837–6849 (2001)
22. Philippe, P., Bideau, D.: Numerical model for granular compaction under vertical tapping. Phys. Rev. E **63**, 051304 (2001)
23. Madadi, M., Tsoungui, O., Lätzel, M., Luding, S.: On the fabric tensor of polydisperse granular materials in 2D. Int. J. Solids Struct. **41**, 2563–2580 (2004)